ACS Macro Letters

Letter

pubs.acs.org/macroletters

# Rational Design of Thermally Stable, Bicontinuous Donor/Acceptor Morphologies with Conjugated Block Copolymer Additives

Dylan Kipp,[†] Jorge Mok,[‡] Joseph Strzalka,[§] Seth B. Darling,[∥,⊥] Venkat Ganesan,[†] and Rafael Verduzco*[,‡,#]

[†]Department of Chemical Engineering, University of Texas at Austin, Austin, Texas 78712, United States

[‡]Department of Chemical and Biomolecular Engineering and [#]Department of Materials Science and NanoEngineering, Rice University, Houston, Texas 77005, United States

[§]X-ray Science Division, Advanced Photon Source, and [∥]Center for Nanoscale Materials, Argonne National Laboratory, Argonne, Illinois 60439, United States

[⊥]Institute for Molecular Engineering, University of Chicago, Chicago, Illinois 60637, United States

Supporting Information

**ABSTRACT:** The bicontinuous microemulsion (B$\mu$E) phase is an equilibrium morphology characterized by cocontinuous domains, high interfacial areas, and nanoscale domain dimensions. These characteristics make the B$\mu$E potentially suitable for use in organic photovoltaic applications. Here, we use a combination of simulations and experiments to investigate the equilibrium morphologies formed by a ternary blend of conjugated polymer, all-conjugated diblock copolymer, and fullerene derivative PCBM. Using coarse-grained simulations, we identify the blend compositions that are most likely to result in donor/acceptor morphologies resembling the B$\mu$E. Experimentally, we probe these compositions through transmission electron microscopy and grazing-incidence X-ray scattering measurements. We demonstrate that all-conjugated block copolymer additives can be used to produce thermally stable, cocontinuous donor/acceptor morphologies at higher additive contents and longer annealing times than previously reported. These results demonstrate that conjugated BCP compatibilizers can be used as a means to achieve equilibrium, cocontinuous morphologies in donor/acceptor blends.

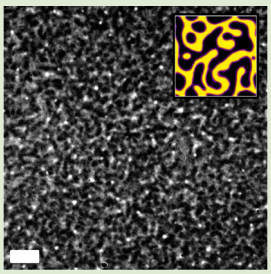

Organic solar cells (OSCs) based on the conjugated polymer/PCBM blend boast the shortest expected energy payback time among various photovoltaic technologies.[1] However, two of the primary challenges still limiting the marketability of these devices are (i) the lower device efficiency of the OSC relative to the more conventional silicon-based solar cell and (ii) the long-term thermal instability of the device active layer.[2] Indeed, high performance organic solar cells are typically based on kinetically determined morphologies that degrade upon thermal annealing. In contrast, the achievement of equilibrium donor/acceptor morphologies with the characteristics known to yield high device performance could provide an effective form of solar energy harvesting that remains stable over time.

The bicontinuous microemulsion (B$\mu$E)[3−5] is a well-known equilibrium morphology characterized by cocontinuous domains, high interfacial areas, and nanoscale domain dimensions. These characteristics make the B$\mu$E potentially suitable for use as an "ideal" device active layer in organic photovoltaic applications. In the context of polymeric systems, the B$\mu$E is often achieved by the addition of a diblock copolymer compatibilizer (AB) to a blend of two immiscible homopolymers (A and B).[4] Previous studies have demonstrated the rational design of B$\mu$Es using a variety of flexible polymeric materials.[6−8] Unfortunately, these *flexible* polymer materials are typically inappropriate for use in OSC active layers. However, recent simulations by Kipp et al. demonstrated that diblock copolymer compatibilizers can also be used as an additive in *semiflexible* polymer/solvent blends to achieve B$\mu$E phases (the authors studied this system as a model for the conjugated polymer/PCBM system often used in OSCs).[9,10] Whether morphologies like those resulting from the simulations are accessible to the experiments remains an outstanding question.

In this work, we use a combination of simulations and experiments to investigate the equilibrium-like morphologies formed by a ternary blend of conjugated polymer, all-conjugated diblock copolymer, and spherical fullerene molecules. Specifically, we seek to address if the combination of simulations and experiments can guide the rational design of thermally stable morphologies with characteristics like that of the B$\mu$E in the case of this blend system. We note that some previous works have also investigated the use of copolymer compatibilizer additives in donor/acceptor blends.[11] Broadly, these studies have used the copolymer compatibilizer as a means either to improve the thermal stability of the device active layer[12−16] or to modify the donor/acceptor morphology, thereby leading to increased device efficiency.[17−22] Our approach is unique in that we are investigating near-equilibrium morphologies; consequently, we are able to use *equilibrium*

**Received:** June 20, 2015
**Accepted:** August 4, 2015
**Published:** August 6, 2015

ACS Publications © 2015 American Chemical Society



DOI: 10.1021/acsmacrolett.5b00413
*ACS Macro Lett.* 2015, 4, 867−871

simulation methods as a means to predict phase behavior and to guide the experiments.

As an experimental system of interest, we consider the blend of poly(thieno[3,4-*b*]-thiophene-*co*-benzodithiophene) (PTB7), PTB7-*b*-polynaphthalene diimide (PTB7-*b*-PNDI), and phenyl-C61-butyric acid methyl ester (PCBM). We select this specific blend due to the attractive electronic and morphological characteristics of the blend components. For instance, recent experiments have demonstrated the superior performance of OSCs based on the PTB7/PCBM blend, as indicated by a record power conversion efficiency of 9.2%.[23−25] PNDI has a high electron mobility and can be incorporated at high blend concentrations as a second electron acceptor.

The self-assembly of the experimental system on mesoscopic length scales is governed primarily by the compositional interactions between and the crystalline ordering of the PTB7, PNDI, and PCBM blend components. These elements can be incorporated in a coarse-grained model of the system in which the conjugated polymers are treated as semiflexible chains and the PCBM molecule is treated as an explicit solvent. In recent works, Kipp et al. used the framework of single chain in mean field (SCMF) simulations[26,27] to study the phase behavior of such a model system.[9,10] Their investigations demonstrated that the influence of the compositional interactions on the equilibrium phase behavior is generally much stronger than the influence of the orientational ordering, and that the locations of the channels of B$\mu$E depend only slightly on the conjugated polymer rigidity. The primary influence of rigidity and orientational interactions was observed to be on the spinodal lines. In contrast, the blend compositions corresponding to the various phase transitions were found to depend more sensitively on the composition of the BCP and on the relative values of the Flory−Huggins interaction parameters. Motivated by these findings, in this work, we utilize a similar coarse-grained model that incorporates only the effects of compositional interactions. Explicitly, we consider a blend of flexible homopolymer, flexible diblock copolymer, and solvent (a model of PCBM) as a coarse-grained model of our experimental blend system.

We utilize the framework of SCMF simulations[26,27] along with a design rule to identify the blend formulations that are most likely to form B$\mu$E-like morphologies in experiments.[10] The formation of B$\mu$E morphologies depends on the competition between microphase and macrophase separation that takes place in the vicinity of where the spinodal and the mean field microphase-to-macrophase transition intersect (see Figure 1). In the ternary composition space of a homopolymer, a block copolymer (BCP), and a solvent (PCBM), this intersection constitutes a line that we refer to as the *mean field locus line*. In a previous work, Kipp et al. hypothesized and corroborated by simulations that a wide channel of B$\mu$E phases is most likely to form at those points along the mean field locus line that correspond to the edge of the lamellar phase.[10] Accordingly, we use simulations here to identify those points along the mean field locus line that result in a lamellar phase; these points are likely to yield B$\mu$E phases in experiments.

For our coarse-grained model, we quantify the strength of the Flory−Huggins interactions between blend components using the parameters $\chi_{\mathrm{PTB7-PCBM}}$, $\chi_{\mathrm{PTB7-PNDI}}$, and $\chi_{\mathrm{PNDI-PCBM}}$. We utilize a simple method based on contact angle experiments[28] as a means to measure our $\chi_{ij}$s. Details of the methods used to calculate $\chi_{ij}$ from contact angle measurements are relegated to the Supporting Information.

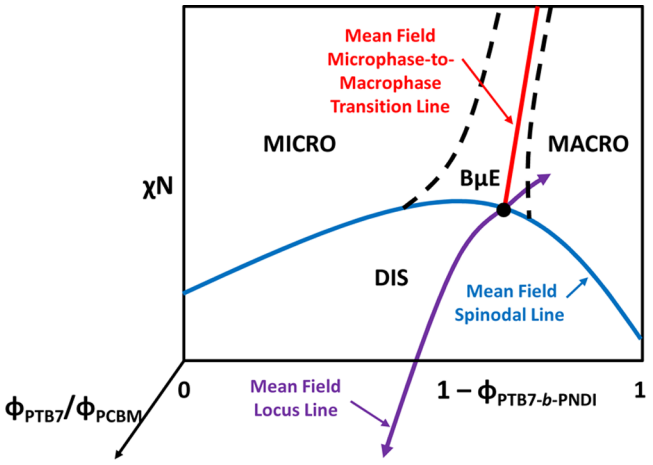


**Figure 1.** Schematic of phase behavior for a ternary blend system of homopolymer, BCP, and solvent (PCBM). The regions labeled MICRO, MACRO, and DIS are regions of thermodynamically stable microphase (lamellar or droplet), macrophase (2-phase or 3-phase coexistence), and compositionally disordered morphologies, respectively. The strength of compositional interactions is measured by the Flory−Huggins parameter, $\chi$. $\phi_i$ indicates the volumetric blend composition of component $i$, where $i$ indicates the homopolymer ($i$ = PTB7), BCP ($i$ = PTB7-*b*-PNDI), or solvent ($i$ = PCBM). For a given ratio $\phi_{\mathrm{PTB7}}/\phi_{\mathrm{PCBM}}$, a mean field spinodal line and microphase-to-macrophase transition line exist in $[1 - \phi_{\mathrm{PTB7-}b\mathrm{-PNDI}} = \phi_{\mathrm{PTB7}} + \phi_{\mathrm{PCBM}}, \chi N]$ space (these are shown as the blue and red lines in the schematic). The mean field locus line is defined as the intersection of the spinodal plane and the microphase-to-macrophase transition plane that results by varying $\phi_{\mathrm{PTB7}}/\phi_{\mathrm{PCBM}}$. This schematic was adapted from Fredrickson and Bates.[6]

The measured values of $\chi_{ij}$ are provided in Table 1. Given the values of the $\chi_{ij}$s, the BCP is not likely to act as a compatibilizer

**Table 1. Flory-Huggins Interaction Parameters for Homopolymer/BCP/Solvent Blend System**

| | |
|---|---|
| $\chi_{\mathrm{PTB7-PNDI}}$ | 1.20 |
| $\chi_{\mathrm{PTB7-PCBM}}$ | 0.77 |
| $\chi_{\mathrm{PNDI-PCBM}}$ | 3.36 |

in the conventional sense by reducing the interfacial tension between domains rich in PTB7 homopolymers and domains rich in PCBM. Rather, because $\chi_{\mathrm{PTB7-PCBM}} < \chi_{\mathrm{PNDI-PCBM}}$, the PCBM is likely to preferentially distribute to the PTB7 and away from the PNDI. However, the results of our previous simulation studies indicate that B$\mu$E-like morphologies should still be accessible for this combination of $\chi_{ij}$s on the condition that the microphase-to-macrophase transition is a transition directly to the lamellar phase.[10] Under these conditions, we anticipate lamellar morphologies of domains rich in PNDI and domains rich in PTB7 and PCBM to form on the condition that $\phi_{\mathrm{PNDI}} \approx \phi_{\mathrm{PTB7}} + \phi_{\mathrm{PCBM}}$ (where $\phi_i$ indicates the volume fraction of component $i$ in the blend). It is necessary to use a BCP with a high PNDI content to satisfy such a condition. We synthesized such a BCP, and the characterization of our materials is provided in Table 2. Further details of the material synthesis and characterization are provided in the Supporting Information.

Figure 2 summarizes the phase behavior of our coarse-grained model as evaluated using SCMF simulations: Figure 2A is a phase diagram and Figure 2B−E show the distribution of



DOI: 10.1021/acsmacrolett.5b00413
*ACS Macro Lett.* 2015, 4, 867−871

**Table 2. Material Characterization**[a]

| material | $M_w$ (kDa) | PDI | $N_{PTB7}$ | $N_{PNDI}$ |
|---|---|---|---|---|
| PTB7 | 16.07 | 2.14 | 21 | 0 |
| PTB7-*b*-PNDI | 82.97 | 4.57 | 11 | 76 |

[a] $M_w$ is the weight-average molecular weight; PDI is the polydispersity index $M_w/M_n$, where $M_n$ is the number-average molecular weight; $N_{PTB7}$ and $N_{PNDI}$ are the number of reference volumes of PTB7 and PNDI repeat units making up each polymer chain.

PNDI, PCBM, and PTB7 units for a morphology resembling the B$\mu$E. At small $\phi_{PTB7-b-PNDI}$ and regardless of the ratio $\phi_{PTB7}/(\phi_{PCBM} + \phi_{PTB7})$, the PNDI-content of the blend formulation is low, and the simulations result in PNDI-rich droplet domains suspended in a continuous domain rich in PTB7 and PCBM. In contrast, at high $\phi_{PTB7-b-PNDI}$, the PNDI content of the blend is high, and the simulations result in a PNDI-rich continuous domain surrounding droplets rich in PTB7 and PCBM. Lamellar morphologies result only in the case of intermediate $\phi_{PTB7-b-PNDI}$ where the morphology transitions from droplets of PNDI to a continuous PNDI phase. The mean field locus line falls within the phase space of lamella only in the cases of $\phi_{PTB7}/(\phi_{PCBM} + \phi_{PTB7}) \geq 0.65$. These results suggest that a channel of B$\mu$E is most likely to form at higher values of $\phi_{PTB7}/(\phi_{PCBM} + \phi_{PTB7})$. However, the formation of B$\mu$E morphologies depends on thermal fluctuations that are strongest at high solvent concentrations. Accordingly, we conclude that B$\mu$E morphologies are most likely to form in the case of $\phi_{PTB7}/(\phi_{PCBM} + \phi_{PTB7}) = 0.65$; this is the smallest $\phi_{PTB7}/(\phi_{PCBM} + \phi_{PTB7})$ (and, hence, the strongest strength of thermal fluctuations) for which the mean field locus line represents a transition to the lamellar phase. Based on the simulations, we would anticipate B$\mu$E-like morphologies to form in experiments for the blend composition $\phi_{PTB7}/(\phi_{PCBM} + \phi_{PTB7}) = 0.65$ and $\phi_{PTB7-b-PNDI} \approx 0.5$.

Motivated by the simulation results summarized above, we produced spin-cast thin films based on various blend compositions in which the ratio $\phi_{PTB7}/(\phi_{PCBM} + \phi_{PTB7})$ is held constant at 0.65. To access equilibrium-like morphologies, we thermally anneal the spin-cast films at elevated temperatures (250 °C) for a period of 7 days. Films were characterized by a combination of transmission electron microscopy (TEM) (see Figure 3) and grazing-incidence small-angle X-ray scattering (GISAXS; see Figure 4). GISAXS measurements were performed at beamline 8-ID-E of the Advanced Photon Source. Details of the thin film preparation procedures are deferred to the Supporting Information. All morphology results provided in this article are for annealed films, but we provide TEM micropgraphs of the as-cast films in the Supporting Information (see Figures S1 and S2).

In the following discussion, we describe the results from the experiments and compare them to the simulations. In the cases of $\phi_{PTB7-b-PNDI} = 0.3$ and $\phi_{PTB7-b-PNDI} = 0.4$, the simulations predict a morphology characterized by PNDI droplets dispersed randomly throughout a matrix of PTB7 and PCBM (Figure 2). In the TEM images (Figure 3A,B), we observe irregularly placed white droplets in a black continuous domain. The darker color regions indicate the preferential distribution of the PCBM material. Further, the results of the simulations and the relative ordering of the $\chi_{ij}$s from Table 1 indicate that the white droplets are rich in PNDI (poor in PCBM), while the black continuous domain is PTB7 and PCBM intermixed. In transitioning from $\phi_{PTB7-b-PNDI} = 0.3$ to $\phi_{PTB7-b-PNDI} = 0.4$, we observe that the PNDI domains become more string-like, interconnected, and large in size. In the GISAXS profiles (Figure 4), this transition manifests as a shift in the characteristic feature from $q_y \approx 0.00252$ Å$^{-1}$ to $q_y \approx 0.00192$ Å$^{-1}$, indicating a change in feature size from ≈250 to ≈330 nm. These experimental results agree with the simulations, which predict that the PNDI droplets should elongate and grow to more closely resemble lamella sheets as a result of increasing $\phi_{PTB7-b-PNDI}$ from below the transition from PNDI droplets to lamella.

In the case of $\phi_{PTB7-b-PNDI} = 0.5$, the simulations predict a lamellar morphology with characteristics like that of the B$\mu$E. We observe in the TEM image (Figure 3C) a cocontinuous morphology of white and black domains that undulate and interweave; this interweaving is a key characteristic of the B$\mu$E[3] that indicates that the morphology achieved may be cocontinuous in all three spatial dimensions. In the GISAXS profiles, we observe a characteristic feature that is broad in width at $q_y \approx 0.00103$ Å$^{-1}$, indicating a distribution of domain periodicity up to 600 nm (i.e., the individual black and white domains visible in the TEM image reach up to 300 nm in width according to the GISAXS profile). This broad feature and associated distribution of domain sizes is a second key characteristic of the B$\mu$E phase.[5]

In comparing the results for $\phi_{PTB7-b-PNDI} = 0.5$ to $\phi_{PTB7-b-PNDI} < 0.5$, we observe two important morphological changes: (i) the

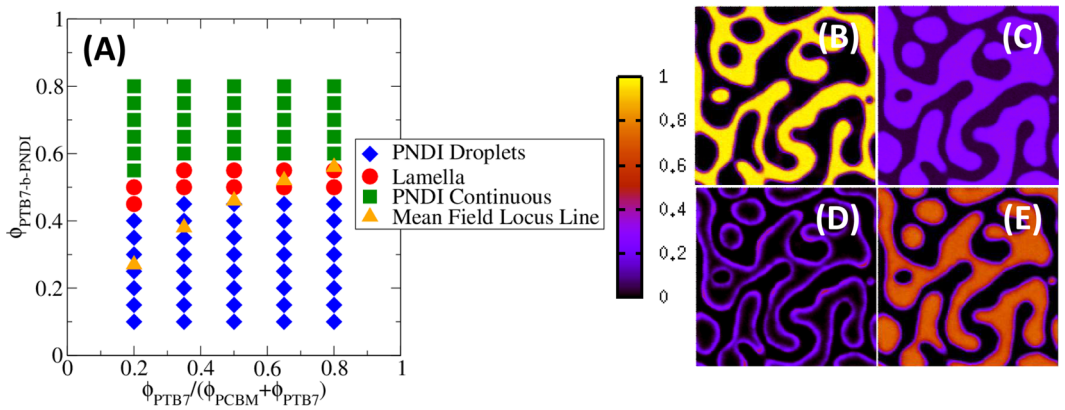


**Figure 2.** Phase behavior of homopolymer/BCP/solvent blend resulting from 2D SCMF simulations. (A) Phase diagram, (B–E) volumetric densities of component units in case of B$\mu$E-like morphology: (B) PNDI, (C) PCBM, (D) PTB7 block of BCP, (E) PTB7 homopolymer.



DOI: 10.1021/acsmacrolett.5b00413
*ACS Macro Lett.* 2015, 4, 867–871

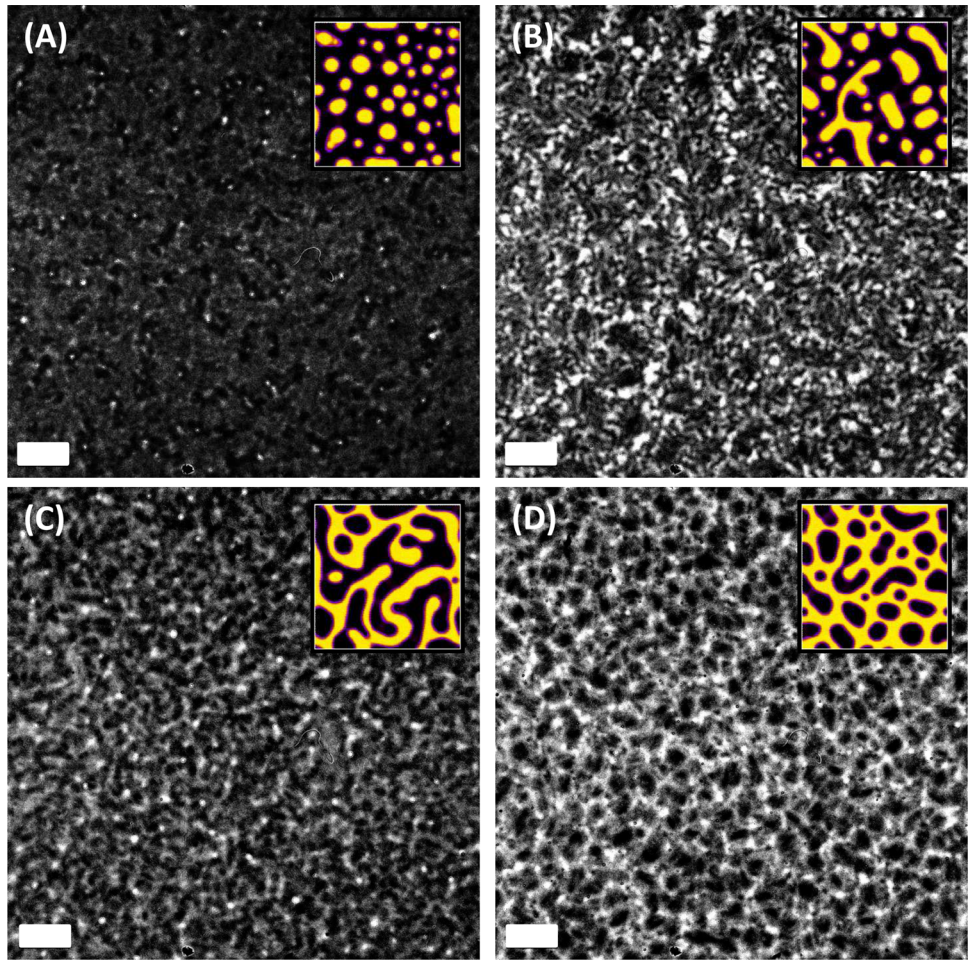


**Figure 3.** Cross-sectional TEM images of thermally annealed thin films with $\phi_{PTB7}/(\phi_{PTB7} + \phi_{PCBM}) = 0.65$: (A) $\phi_{PTB7\text{-}b\text{-}PNDI} = 0.3$, (B) $\phi_{PTB7\text{-}b\text{-}PNDI} = 0.4$, (C) $\phi_{PTB7\text{-}b\text{-}PNDI} = 0.5$, (D) $\phi_{PTB7\text{-}b\text{-}PNDI} = 0.6$. In all cases, $\phi_{PTB7\text{-}b\text{-}PNDI} = 1.0 - \phi_{PTB7} - \phi_{PCBM}$. The scale bar is 1 $\mu$m. The insets show the volumetric density of PNDI resulting from SCMF simulations to match the experiments.

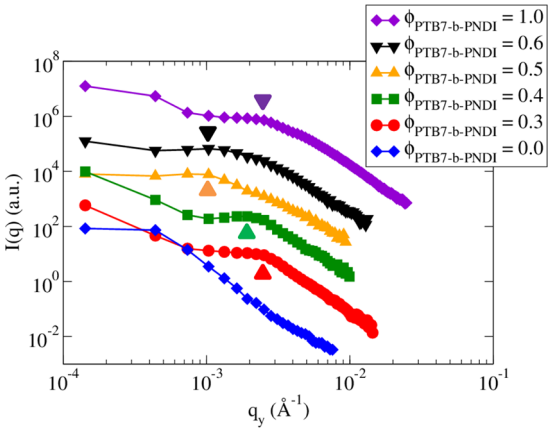


**Figure 4.** GISAXS profiles of thermally annealed thin films. In all cases, $\phi_{PTB7}/(\phi_{PTB7} + \phi_{PCBM}) = 0.65$ and $\phi_{PTB7\text{-}b\text{-}PNDI} = 1.0 - \phi_{PTB7} - \phi_{PCBM}$. GISAXS intensities are offset for clarity. Characteristic features apparent in the profiles are indicated by solid triangles.

large continuous black domains that are visible in the TEM images for the cases of $\phi_{PTB7\text{-}b\text{-}PNDI} < 0.5$ are not apparent in the case of $\phi_{PTB7\text{-}b\text{-}PNDI} = 0.5$, and (ii) the upturn in the low-$q$ scattered intensity that characterizes the GISAXS profiles in the cases of $\phi_{PTB7\text{-}b\text{-}PNDI} < 0.5$ does not characterize the case of $\phi_{PTB7\text{-}b\text{-}PNDI} = 0.5$. Combined, these morphological changes indicate the suppression of macroscopic phase separation at $\phi_{PTB7\text{-}b\text{-}PNDI} = 0.5$. In comparison to the simulations, the onset of the microphase-to-macrophase transition and the transition from PNDI droplets to lamella at $\phi_{PTB7\text{-}b\text{-}PNDI} = 0.5$ agrees with the predictions and suggests that a morphology with characteristics like that of a B$\mu$E is likely to form.

In the TEM image for $\phi_{PTB7\text{-}b\text{-}PNDI} = 0.6$ (Figure 3D), we observe a morphology of black droplet domains (rich in PTB7/PCBM) suspended in a white continuous domain (rich in PNDI). This experimental result agrees with the simulations, which predict a transition from lamellar morphologies to PNDI continuous morphologies at $\phi_{PTB7\text{-}b\text{-}PNDI} = 0.6$. At a composition above the microphase-to-macrophase transition, the placement of black droplets within the white matrix is more regular as compared to the randomly dispersed white droplets that form in the cases of $\phi_{PTB7\text{-}b\text{-}PNDI} < 0.5$. We observe in the GISAXS profile a characteristic feature at $q_y \approx 0.00103$ Å$^{-1}$ or ≈600 nm in size. More generally, the peak in characteristic feature size located at $\phi_{PTB7\text{-}b\text{-}PNDI} = 0.5$, as observed in the GISAXS profiles agrees well with the simulation results (see the insets in Figure 2A–D).

In order to further bolster (i) the interpretation of the results presented in this main text and (ii) the validity of our simulation method for predicting phase behavior, we investigated the equilibrium phase behavior of a second set of homopolymer and block copolymer materials. The materials



DOI: 10.1021/acsmacrolett.5b00413
ACS Macro Lett. 2015, 4, 867–871

characterization and morphology results are presented in Table S2 and Figure S3 of the Supporting Information, respectively. For this study, we utilized a BCP with a lower PNDI composition as compared to the BCP studied in the main text and presented in Table 2. Consistent with the predictions of the simulations, we observed the formation of spherical domains roughly 200 nm in size. The simulations were successful in predicting the phase behavior, including such important transitions as the compositional order−disorder transition and the microphase-to-macrophase transition.

To summarize this article, we demonstrated the rational design of donor/acceptor morphologies based on the PTB7/PTB7-*b*-PNDI/PCBM blend using a combination of simulations and experiments. The B$\mu$E-like morphology (resulting in experiments and described above for the case of $\phi_{\text{PTB7-}b\text{-PNDI}} = 0.65$) has promise as an OSC active layer because it is characterized by cocontinuous and thermally stable donor and acceptor domains of roughly 100−300 nm in size. B$\mu$E-like morphologies with smaller domain sizes could also be designed by using polymer components characterized by smaller degrees of polymerization or varying the composition of the BCP to target B$\mu$E-like morphologies in other areas of the blend composition space.[9] In future studies, we intend to characterize the device efficiencies of such B$\mu$E-like morphologies and investigate if they do, in fact, lead to higher device performance.

## ■ ASSOCIATED CONTENT

### Supporting Information

The mathematical formulation of the model, a method for approximating $\chi_{ij}$s from contact angle measurements, the specifics of the material synthesis, and additional TEM results. The Supporting Information is available free of charge on the ACS Publications website at DOI: 10.1021/acsmacrolett.5b00413.

(PDF)

## ■ AUTHOR INFORMATION


### Corresponding Author

*E-mail: rafaelv@rice.edu.


### Notes

The authors declare no competing financial interest.

## ■ ACKNOWLEDGMENTS

We acknowledge Prof. Chris Ellison for useful discussions. This work was supported in part by grants from the Robert A. Welch Foundation (Grant F1599), the National Science Foundation (CBET-1264583 and NSF-1264703), and the U.S. Army Research Office (W911NF-13-1-0396). The authors acknowledge the Texas Advanced Computing Center (TACC) at The University of Texas at Austin for providing computing resources that have contributed to the research results reported within this paper. This work was supported in part by the U.S. Department of Energy, Office of Science, Office of Basic Energy Sciences in the Institute for Molecular Engineering, the Center for Nanoscale Materials, and the Advanced Photon Source at Argonne National Laboratory under Contract No. DE-AC02-06CH11357.

## ■ REFERENCES


(1) Darling, S. B.; You, F. *RSC Adv.* **2013**, *3*, 17633−17648.
(2) Thompson, B. C.; Fréchet, J. M. J. *Angew. Chem., Int. Ed.* **2008**, *47*, 58−77.
(3) Bates, F. S.; Maurer, W. W.; Lipic, P. M.; Hillmyer, M. A.; Almdal, K.; Mortensen, K.; Fredrickson, G. H.; Lodge, T. P. *Phys. Rev. Lett.* **1997**, *79*, 849−852.
(4) Hillmyer, M. A.; Maurer, W. W.; Lodge, T. P.; Bates, F. S.; Almdal, K. *J. Phys. Chem. B* **1999**, *103*, 4814−4824.
(5) Morkved, T. L.; Stepanek, P.; Krishnan, K.; Bates, F. S.; Lodge, T. P. *J. Chem. Phys.* **2001**, *114*, 7247.
(6) Fredrickson, G. H.; Bates, F. S. *J. Polym. Sci., Part B: Polym. Phys.* **1997**, *35*, 2775−2786.
(7) Ellison, C. J.; Meuler, A. J.; Qin, J.; Evans, C. M.; Wolf, L. M.; Bates, F. S. *J. Phys. Chem. B* **2009**, *113*, 3726−3737.
(8) Pandav, G.; Ganesan, V. *Macromolecules* **2013**, *46*, 8334−8344.
(9) Kipp, D.; Ganesan, V. *J. Phys. Chem. B* **2014**, *118*, 4425−4441.
(10) Kipp, D.; Wodo, O.; Ganapathysubramanian, B.; Ganesan, V. *ACS Macro Lett.* **2015**, *4*, 266−270.
(11) Yuan, K.; Chen, L.; Chen, Y. *Polym. Int.* **2014**, *63*, 593−606.
(12) Sivula, K.; Ball, Z.; Watanabe, N.; Fréchet, J. *Adv. Mater.* **2006**, *18*, 206−210.
(13) Lee, J. U.; Jung, J. W.; Emrick, T.; Russell, T. P.; Jo, W. H. *J. Mater. Chem.* **2010**, *20*, 3287−3294.
(14) Yuan, K.; Chen, L.; Chen, Y. *Polym. Int.* **2014**, *63*, 593−606.
(15) Lee, Y.-H.; Chen, W.-C.; Chiang, C.-J.; Kau, K.-C.; Liou, W.-S.; Lee, Y.-P.; Wang, L.; Dai, C.-A. *Nano Energy* **2015**, *13*, 103−116.
(16) Palermo, E. F.; Darling, S. B.; McNeil, A. J. *J. Mater. Chem. C* **2014**, *2*, 3401−3406.
(17) Yang, C.; Lee, J. K.; Heeger, A. J.; Wudl, F. *J. Mater. Chem.* **2009**, *19*, 5416−5423.
(18) Tsai, J.-H.; Lai, Y.-C.; Higashihara, T.; Lin, C.-J.; Ueda, M.; Chen, W.-C. *Macromolecules* **2010**, *43*, 6085−6091.
(19) Ren, G.; Wu, P.-T.; Jenekhe, S. A. *Chem. Mater.* **2010**, *22*, 2020−2026.
(20) Sun, Z.; Xiao, K.; Keum, J. K.; Yu, X.; Hong, K.; Browning, J.; Ivanov, I. N.; Chen, J.; Alonzo, J.; Li, D.; Sumpter, B. G.; Payzant, E. A.; Rouleau, C. M.; Geohegan, D. B. *Adv. Mater.* **2011**, *23*, 5529−5535.
(21) Mulherin, R. C.; Jung, S.; Huettner, S.; Johnson, K.; Kohn, P.; Sommer, M.; Allard, S.; Scherf, U.; Greenham, N. C. *Nano Lett.* **2011**, *11*, 4846−4851. PMID: 21985612.
(22) Chen, J.; Yu, X.; Hong, K.; Messman, J. M.; Pickel, D. L.; Xiao, K.; Dadmun, M. D.; Mays, J. W.; Rondinone, A. J.; Sumpter, B. G.; Kilbey II, S. M. *J. Mater. Chem.* **2012**, *22*, 13013−13022.
(23) He, Z.; Zhong, Z.; Su, S.; Xu, M.; Wu, H.; Cao, Y. *Nat. Photonics* **2012**, *6*, 591−595.
(24) Liang, Y.; Xu, Z.; Xia, J.; Tsai, S.-T.; Wu, Y.; Li, G.; Ray, C.; Yu, L. *Adv. Mater.* **2010**, *22*, E135−E138.
(25) Chen, W.; Xu, T.; He, F.; Wang, W.; Wang, C.; Strzalka, J.; Liu, Y.; Wen, J.; Miller, D. J.; Chen, J.; Hong, K.; Yu, L.; Darling, S. B. *Nano Lett.* **2011**, *11*, 3707−3713.
(26) Müller, M.; Smith, G. D. *J. Polym. Sci., Part B: Polym. Phys.* **2005**, *43*, 934−958.
(27) Daoulas, K. C.; Müller, M. *J. Chem. Phys.* **2006**, *125*, 184904.
(28) Nilsson, S.; Bernasik, A.; Budkowski, A.; Moons, E. *Macromolecules* **2007**, *40*, 8291−8301.




DOI: 10.1021/acsmacrolett.5b00413
*ACS Macro Lett.* 2015, 4, 867−871